actuators

MDPI

Article

Simultaneous Identification of Free and Supported Frequency Response Functions of a Rotor in Active Magnetic Bearings

Michael Kreutz [1,2,*], Johannes Maierhofer [1,2], Thomas Thümmel [1,2] and Daniel J. Rixen [1,2]

[1] Chair of Applied Mechanics, Department of Mechanical Engineering, TUM School of Engineering & Design, Technical University of Munich, 85748 Garching, Germany; j.maierhofer@tum.de (J.M.); thuemmel@tum.de (T.T.); rixen@tum.de (D.J.R.)

[2] Munich Institute of Robotics and Machine Intelligence (MIRMI), Technical University of Munich, 80992 München, Germany

* Correspondence: m.kreutz@tum.de

Abstract: Frequency response functions (FRFs) of rotor systems can be used as indicator functions for condition monitoring. Component-wise FRFs are of high interest to locate errors in the case of defects. To enable continuous monitoring, measurements should be taken during operation. This contribution shows methods of using active magnetic bearings (AMBs) for simultaneously determining different FRFs of a rotor system. The AMBs, in addition to supporting the rotor, are used simultaneously as sensors and actuators. Two different types of FRFs, namely, the one associated with the free rotor and with the supported rotor can be determined from a single experiment. This procedure does not need any change in the assembly because the AMBs are simultaneously used as bearing and excitation device. Considering as excitation the total bearing force of the AMBs results in the FRF of the free rotor. The FRF of the supported system is determined by considering a perturbation force only, which is applied on top of the controlled AMB force. As a showcase, an academic rotor test rig is used with and without rotation to verify the applicability of the method. To evaluate and interpret the results of the experiments, a numerical model of the rotor using finite-element formulations is used.

Keywords: magnetic bearings; frequency response; identification; substructuring

Citation: Kreutz, M.; Maierhofer, J.; Thümmel, T.; Rixen, D.J. Simultaneous Identification of Free and Supported Frequency Response Functions of a Rotor in Active Magnetic Bearings. *Actuators* **2022**, *11*, 144. https://doi.org/10.3390/act11060144

Academic Editors: Richard M. Stephan, Afonso Celso Del Nero Gomes and José Andrés Santisteban

Received: 27 April 2022
Accepted: 25 May 2022
Published: 28 May 2022

Publisher's Note: MDPI stays neutral with regard to jurisdictional claims in published maps and institutional affiliations.

1. Introduction

Condition monitoring compares a rotor system's actual behavior with a desired or normal behavior using indicators to detect faults. In [1], multiple rotor faults are described using minimal models. Displacement and force orbits are used as indicator functions that are used in combination with models for different rotor faults. Indicator functions can be, for example, frequency response functions (FRFs) or modal parameters. Mechanical FRFs $\boldsymbol{H}(\omega)$ are defined as the linear relationship between harmonic forces $\boldsymbol{F}(\omega)$ and harmonic responses $\boldsymbol{X}(\omega)$ (displacement, velocity or acceleration), which depend on the excitation frequency ω, cf. [2]:

$$\boldsymbol{X}(\omega) = \boldsymbol{H}(\omega)\,\boldsymbol{F}(\omega). \tag{1}$$

Obtaining the FRFs in simulation models requires low effort, as long as the model size is not too large. For a symmetric rotor, considering gyroscopic effects, the FRFs for a rotational speed Ω can be obtained by, cf. [3]:

$$\boldsymbol{H}(\omega) = \left(-\omega^2\boldsymbol{M} + i\omega(\boldsymbol{C} + \boldsymbol{G}(\Omega)) + \boldsymbol{K}\right)^{-1} \tag{2}$$

with the system's mass, damping, gyroscopic and stiffness matrix represented as $\boldsymbol{M}$, $\boldsymbol{C}$, $\boldsymbol{G}$ and $\boldsymbol{K}$ respectively.

To estimate the FRF from a set of given input (force) to output (response) time-signals, a number of algorithms, based on fast Fourier transforms, exist. Experimentally determining

the FRFs of rotating systems is a special challenge. The FRFs obtained from measurement are often used in experimental modal analysis (EMA) to determine the modal properties of the system.

In order to measure the FRFs of a system, typically, its operation must be stopped. The system must be instrumented by exciters and sensors. Stopping the system's operation and performing the tests takes a lot of time and effort. So, this is not feasible for condition monitoring.

In this contribution, the AMBs are used as combined exciters and sensors while still being used as bearings. This enables us to measure the FRFs of the rotor system during operation and thus avoids the need to stop its operation.

The force in the active magnetic bearings for normal operation is set by a current from its PID-controller. To measure the system's FRFs, an additional excitation current is added to the controller current. This is called the excitation force. The total force includes both the controller and the additional excitation force.

The excitation force and the total force in the bearing is estimated by a linear current–force relationship. With this, it is possible to determine the FRFs of the supported system and of the free rotor in a single measurement run. Thus, FRFs can be used for a continuous condition monitoring of the rotor system. Knowing both the free and the supported FRFs of the rotor is especially useful for localizing faults in the rotor system, as the bearing effects can be separated from the rotor effects in the different FRFs.

Many publications have treated the identification of bearing parameters. In the review paper [4], a comprehensive summary of identification techniques using vibration signals is given. Different excitation sources can be used to obtain the necessary vibration signals. For example, Refs. [5–7] use the excitation from a mass unbalance to determine the bearing parameters. Impact excitation is commonly used in structural dynamics identification but can also be used for rotating systems. In [8], an impact excitation is applied through an intermediate ball bearing on a rotating disc. In [9], impact testing is applied to a non-rotating rotor in magnetic bearings to obtain FRFs, which are used to improve the AMBs' control. A natural idea in rotor systems with AMBs is to use them for an excitation of the system. An overview of the state-of-the-art AMBs can be found in [10], where there is a section dedicated to condition monitoring using AMBs.

An overview of strategies to measure FRFs of rotating systems have been proposed in the BRITE/MARS project [11], also discussed in [3]. In these publications, active magnetic bearings (AMBs) are used as an excitation system in addition to the existing support in ball bearings. Similarly, in [12], a bearingless motor is used to excite a system with oil-film bearings. Related work can also be found in [13], where the parameters of the oil-film bearings and the bearingless motor are identified through a regression by varying unbalance and controller parameters. In [14], an excitation device similar to magnetic bearings is used to identify the dynamics of a machine tool spindle assembly. In [15], an approach for combining the AMB's control system with a MIMO identification procedure to obtain a state-space model is given for systems with real poles. In [16,17], a method to combine the magnetic bearing's support with an additional excitation is given. This is similar to the method applied in this contribution. In [18], an approach of using AMBs to perform EMA of the supported rotor system using an external commercial modal analysis system was shown for the levitating but non-rotating rotor. Furthermore, [16] discusses the possibility to measure the FRF of the free rotor in AMBs but unfortunately does not give results. In the aforementioned publications, except for [16], the FRF of the free rotor could not be measured.

In this contribution, the FRFs of the free and supported rotor can be measured simultaneously with one setup that is suitable for practical applications, see also Section 2.4. The excitation is applied via the bearings, using an additional excitation current that is added to the AMBs' controller currents. The combination of the excitation and bearing task in the magnetic bearing enables us to measure the FRFs of different theoretical system configurations in a single experiment by considering different force signals, which has not

been shown in the literature. The basic idea can be summarized as follows: Considering only the excitation force, which is a perturbation added to the controlled bearing force, the FRF of the supported rotor is obtained. Considering the total force, namely, the sum of contributions from the controller and from the additional excitation, gives the FRF of the free rotor. Here, we want to use a simple implementation of a standard MIMO excitation signal, e.g., burst random excitation, which can be found in text books about EMA, for example, in [2] (p. 323ff). We also want to give an intuitive interpretation of the results to understand how AMBs can be used to obtain different FRFs of one system in a single experiment.

The approach is applied to an academic test rig with and without rotation. First, the methodology is presented in Section 2 with the academic test rig as an example. The academic test rig, the experimental procedure, and the simulation model are outlined, and requirements for applying the methodology to a practical application are discussed. Results obtained with the proposed approach for a non-rotating system are given and interpreted in Section 3. The method is then also applied to a rotating system in Section 4. A short outlook on how to estimate the bearing dynamics from the obtained FRFs is given in Section 5. In the end, a short summary and conclusions of the contribution are given.

2. Methodology

The methodology underlying in this contribution is described in this section, using the academic test rig as application example.

2.1. Test Rig

The magnetic bearing test rig at the Chair of Applied Mechanics of the Technical University of Munich is used as an example of a levitating rotor in magnetic bearings. In Figure 1, the schematic view of the magnetic bearing test rig is shown. Figure 2 shows a photo of the test rig. A control scheme of the systems is presented in Figure 3. The test rig is also described in [19,20]. The rotor is supported in active magnetic bearings and can be driven by a servo motor, which is coupled to the rotor via a double cardan joint. An inertia disc and two bearing journals are attached to the shaft via cone clamping elements. Back-up bearings are installed in the front and back plate of each magnetic bearing and near the disc. Displacements are measured in orthogonal transverse directions of the shaft on the front and back plate of each magnetic bearing via eddy current sensors. These sensors are used for the AMBs' control systems and for obtaining the FRFs. Measuring the acceleration by adding acceleration sensors to the rotor shaft is not practical because the system should be able to rotate. The rotation angle is measured by a rotary encoder on the motor shaft. Compared to the test rig configuration in [19], the test rig has been improved by applying additional force-torque sensors (piezo force platform Kistler 9129AA) underneath the magnetic bearings. They give an accurate reading of the magnetic bearing ground force, which corresponds to the total force of the bearing. This information is used later for a validation of total bearing force estimated from the AMB signals.

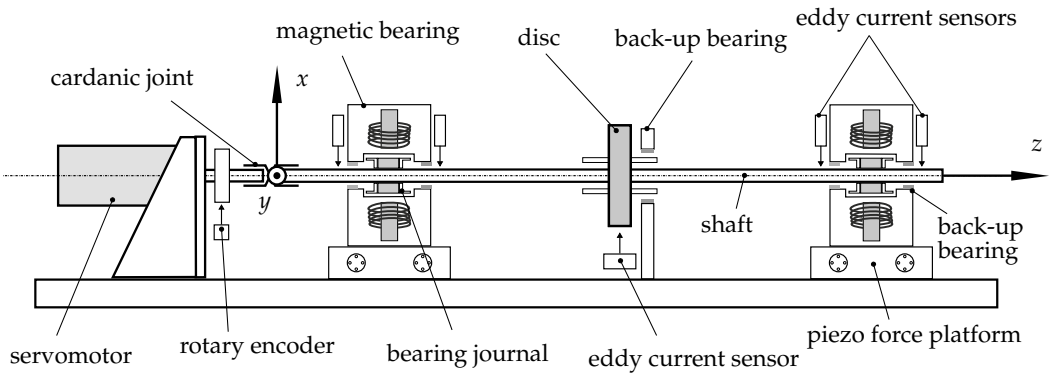

Figure 1. Schematic view of the magnetic bearing test rig, see also [19].

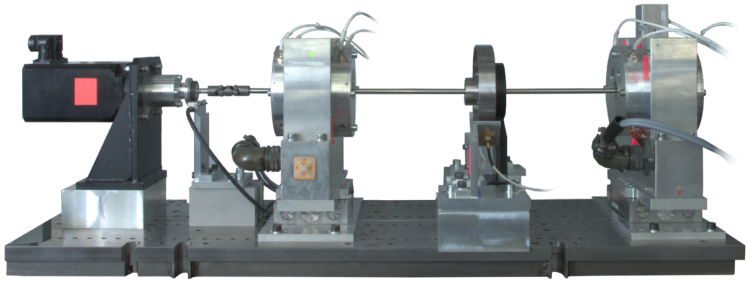

Figure 2. Photo of the magnetic bearing test rig with piezo force platforms.

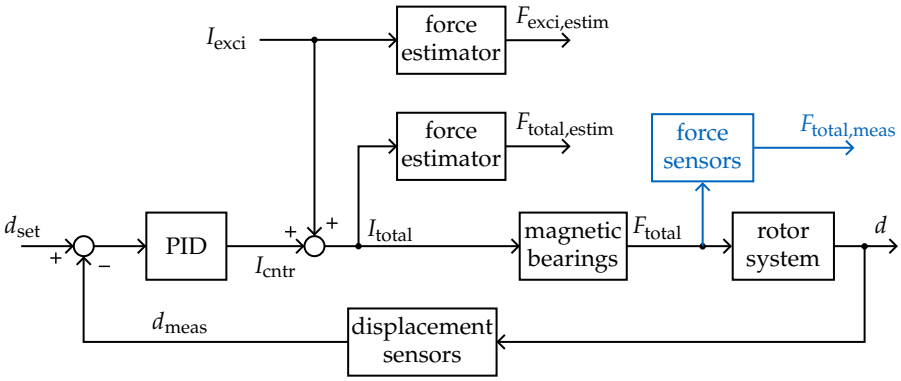

Figure 3. Control scheme including additional excitation.

The position of the rotor in the magnetic bearings is controlled by a PID controller, which uses the position error with the measured displacement d_{meas} as input signal and a control current I_{cntr} as output, see the control scheme in Figure 3. The PID controllers are implemented separately for each direction of each bearing. Only small vibrations inside the bearing are assumed, so that the magnetic force can be considered as linear with respect to the current and independent of the position of the bearing for our example. The non-linearity between the displacement, current and force for this magnetic bearing was investigated in [21].

An additional excitation current I_{exci} can be applied to the magnetic bearings by adding it to the controller current. The force resulting from the excitation current I_{exci} cannot be measured directly. The measured force $F_{total,meas}$ contains both contributions from the controller current I_{cntr} and the excitation current I_{exci}, which cannot be easily separated:

$$F_{total,meas} = f(\, I_{cntr} + I_{exci},\, \ldots). \tag{3}$$

An ideal behavior of the force sensors is assumed ($F_{total} \approx F_{total,meas}$). In order to be able to separate the forces, we assume a linear relationship between the applied current and the resulting force.

$$F = k_i I, \qquad \text{with } k_i = \frac{\sqrt{2}}{4} \cdot 50\,\mathrm{N\,A^{-1}} \approx 17.67\,\mathrm{N\,A^{-1}} \tag{4}$$

The factor k_i was determined in a test rig similar to [21]. The bias current is $I_b = 2.5\,\mathrm{A}$. The magnetic bearings are actuated in a differential driving mode, e.g., [22] (p. 125): the current I is split in current between opposing coils, where one coil is actuated with $I_{coil,1} = I_b + I_{total}/2$ and the opposing coil with $I_{coil,2} = I_b - I_{total}/2$.

The excitation and total force are estimated from Equation (4):

$$F_{exci,estim} = k_i I_{exci}, \qquad F_{total,estim} = k_i I_{total}. \tag{5}$$

They will be used to calculate the FRFs of the supported rotor and the free rotor in this contribution. The force $F_{\text{total,meas}}$ is directly measured by the force platforms. The results using force measured by the force platforms (see Figure 1) are used as comparison to the results using the estimated total force. This is possible in the academic test rig. In an industrial application, adding force sensors adds a lot of cost and complexity and is often not possible due to space restrictions.

2.2. Experimental Procedure

In the experiments, FRF-measurement is performed by using the active magnetic bearings as exciters. The system is controlled by a real-time capable dSPACE-system with an interface to MATLAB/Simulink, which can be used to parameterize the system and read measured values. The experiment uses burst random excitation in x-direction for both AMBs, which consists of 0.5 s excitation using band-limited noise (limited to 250 Hz, amplitude 1.2 A). This is followed by a 1.548 s pause. For information about burst random excitation, see [2] (p. 338). As independent burst random excitations are applied on both AMBs, this is a multiple input multiple output (MIMO) identification procedure. For MIMO identification, it is important that the excitation signals are uncorrelated. The measurement duration is 204.8 s with a sampling rate of 10 kHz. So, the burst signal is repeated 100 times.

The resulting FRFs are calculated from the time data of force and displacement signals by using algorithms included in ABRAVIBE [23], which is a companion software for the text book [2]. The standard H_1-estimator is used because it is widely spread and easily applicable to MIMO identification. A Hanning window (2.048 s long) with 67% overlap is used.

2.3. Simulation Model

To help the interpretation of the experimental results, a numerical model of the test rig is used. The numerical model is built using the open-source rotor simulation toolbox AMrotor, cf. [24,25]. A first model of the system has been built in [20]. This model was the basis for an improved, updated model of the test rig.

The shaft is modeled with Timoshenko beam elements. Viscous Rayleigh damping is assumed. The bearing journals and the discs are modeled as discrete masses including rotational inertia of the components, which was read from the 3D-CAD model. The magnetic bearings are modeled as linear spring-damper elements. The magnetic bearing forces are assumed to be applied to the middle point in each AMB. The cardanic joint is modeled as discrete mass and a linear damper in the transverse direction.

The missing parameters have been identified by a comparison with experimental modal analysis results from impact testing using a commercial modal analysis system. A roving-hammer method was used with one uni-axial acceleration sensor and using the automatic impact hammer AMimpact, cf. [18]. The results of the validation are shown in Figure 4. The missing parameters have been found with the following steps:

a. The rotor is connected to the environment via soft rubber bands to approximate free boundary conditions. This free-floating measurement was used to parameterize and validate the simulation model of the free rotor. The stiffness of the shaft had to be increased. The Young's modulus of the shaft was set to $E = 240\,\text{GPa}$. To account for the additional stiffness of the shaft that is introduced by adding the bearing journals and the disc, the stiffness of the shaft was increased locally in the corresponding regions. This was performed by scaling the stiffness matrices of the elements in the regions of the bearing journals and of the disc before assembly of the finite element model of the rotor. The stiffness at the bearing journals was scaled by 2.5 and at the disc by 2.4. Proportional damping was assumed for the shaft: $\boldsymbol{D} = \alpha_1 \boldsymbol{K} + \alpha_2 \boldsymbol{M}$, with $\alpha_1 = 1.5 \times 10^{-6}\,\text{s}$ and $\alpha_2 = 0.14\,\text{s}^{-1}$. The comparison of the free rotor from impact testing and from the updated simulation model for a driving point shows good agreement. It is shown in Figure 4a. The driving point is located near the right edge of the right bearing journal.

b. After the free-floating measurement, the rotor was mounted in the magnetic bearings of the test rig without assembly of the cardanic joint. In the simulation model, the magnetic bearings are represented by simple linear spring-damper elements. The values for the linear stiffness and damping of the magnetic bearings have been found by fitting the FRF-peak at around 58 Hz, which are mostly determined by the magnetic bearing parameters, as $k_{\mathrm{AMB}} = 1.25 \times 10^5\,\mathrm{N\,m^{-1}}$ and $d_{\mathrm{AMB}} = 60\,\mathrm{N\,s\,m^{-1}}$. The comparison of a driving point FRF is given in Figure 4b. This driving point is located at the right end of the shaft. Mounting the rotor in the magnetic bearings makes measuring the FRFs more difficult using impact excitation. The magnetic bearings introduce noise to the system, and the impact excitation does not give a lot of energy, e.g., compared to a shaker excitation. The effect of the additional noise of the magnetic bearings could be seen in a worse coherence and more noisy FRF data.

c. Then, the cardanic joint is added to the rotor, and the impact testing procedure is repeated. The cardanic joint is needed to impose rotation on the rotor. Adding the cardanic joint shows a clear influence on all modes. It is modeled by an additional mass without rotational inertia at the end of the shaft with $m_{\mathrm{cardan}} = 0.037\,\mathrm{kg}$. The additional damping of the cardanic joint is modeled by a linear damping of $d_{\mathrm{cardan}} = 0.36\,\mathrm{N\,s\,m^{-1}}$. The comparison of a driving point FRF for the systems with the cardanic joint is given in Figure 4c. The driving point located in the same position as in b.

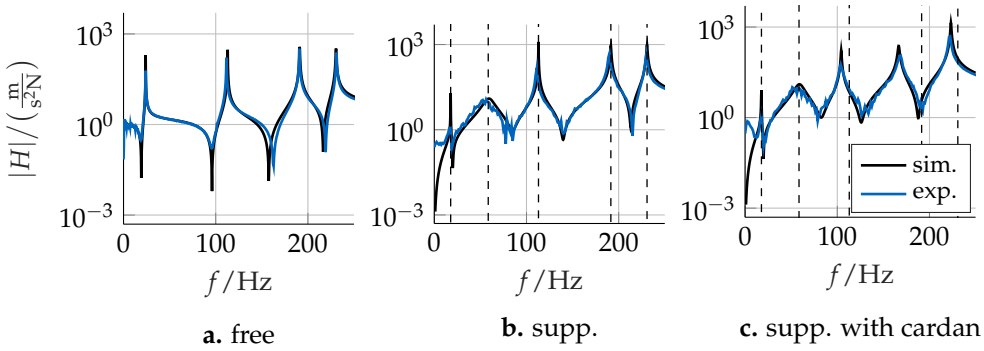

Figure 4. Parametrization of the simulation model by comparison with FRF-results for impact testing with different system setups. The eigenfrequencies of the supported system without the cardanic joint (**b**) are marked by dashed lines to highlight the difference between the system without (**b**) and with (**c**) the cardanic joint.

It can be concluded that parameters have been found for which the simulation model agrees well with the results of the experimental modal analysis using impact excitation. Measurements without the cardanic joint have only been used in this subsection to find the missing parameters of the simulation model.

The simulation model is used to validate the results of the frequency response measurements using the magnetic bearings as exciter. In the following text, all measurements have been performed with the assembled cardanic joint, where the term *free rotor* is used for the free floating rotor with the cardanic joint. The *supported system* is the rotor including the magnetic bearings and the cardanic joint.

2.4. Requirements for Practical Application

In this contribution, the methodology is presented for an academic test rig, but it can also be applied to a more practical application of a rotor in magnetic bearings. The requirement are summarized here.

It must be possible to add an additional excitation current I_{exci} after the controller current I_{cntr} to be able to excite the system. The excitation signal can be very simple, e.g., using white noise. The force applied by the AMBs can be obtained by recording the current commanded by the controllers (I_{exci} and I_{total}). If the constant k_i, see Equation (4), of the AMBs is known,

the forces can be evaluated. Note, however, that FRFs can also be scaled by the currents. The FRFs, then, have different meanings but can still be used similarly to what is done in this contribution for monitoring purposes. For the FRFs of the system, the response of the rotor must be measured. If the AMB's stiffness and damping should be estimated using the decoupling procedure in Section 5, the response signals must be captured in positions very close to the AMBs. Classical AMBs have integrated displacement sensors close to where the force is applied because this signal is necessary for the AMB-controller anyway. The results of a measurement must be recorded, either in the time domain or directly in the frequency domain. Using these results, the FRFs can be computed using a standard FRF-estimation algorithm.

There is also a limit on the stiffness of the AMBs in the practical applications. For the supported system, vibration nodes of the rotor are close to the AMBs. As the AMBs are used as the exciters, problems arise if the vibration nodes are exactly at the AMBs' positions. Excitation in a vibration node means that the corresponding mode is not controllable. This is not a problem for the free rotor's FRF because its vibration nodes are not influenced by the bearings. The stiffer the AMBs act, the harder it is to accurately measure the supported system's FRF.

3. Non-Rotating System

The experimental results for the non-rotating system are obtained in a single measurement and are validated by comparison with simulation results.

3.1. FRF of the Rotor in AMBs Using Additional Excitation Force

In a first step, only the additional excitation force on the AMBs is considered as an input to the FRF calculation algorithm. The excitation force is estimated from the linear static relationship in Equation (5).

Figure 5 shows a simplified model of the resulting system. As only the additional excitation force is considered, the bearings forces are considered as internal forces and thus are included in the dynamic FRF. The abbreviation *supp* is used for the *supported* system.

$$\boldsymbol{X}(\omega) \;=\; \boldsymbol{H}_{\mathrm{supp}}(\omega)\, \boldsymbol{F}_{\mathrm{exci}}(\omega) \tag{6}$$

Figure 6 shows the experimental results for the FRF using only the additional excitation force and compares them with the results from the numerical simulation for the rotor in elastic bearings. It shows the FRF between excitation at the right AMB and the response at the rightmost eddy current sensor. The excitation and response positions are very close, so a behavior similar to a driving point FRF is expected. The experimental and simulation results are clearly similar. The coherence of the experimental FRF is shown in orange. It starts to fall at around 200 Hz because a band-limited noise with a cut-off frequency of 250 Hz was used in the burst random excitation.

The frequency of the peaks in simulation and experiment agree very well. There is a slight difference for the peak at around 165 Hz. The damping of the modes can be qualitatively seen from the sharpness of the peaks. For frequencies above 150 Hz, the simulation's damping is lower than in the experiment. The peak at around 58 Hz is due to the support from the magnetic bearings. The simulation model agrees well for this peak thanks to the model updating procedure, described in Section 2.3. The depicted FRF does not completely show a driving point behavior, which can be seen by the missing anti-resonance between the resonance-peaks at 105 and 168 Hz. This can be observed in both experiments and simulations and is due to the distance between the excitation and response points.

There is an offset in the amplitude between the experimental and simulation results. This is due to imperfections in determining the current–force factor k_i.

The phase of the FRF shows a similar behavior in simulation and experiment. As expected, the phase falls by 180° for resonances and rises by 180° at anti-resonances. The phase of the experimental FRF exhibits, however, a linear drift with frequency. This is due to

effects in the current amplifier, mainly time-delay. These effects are not compensated in the static force estimation using k_i, see Equation (4).

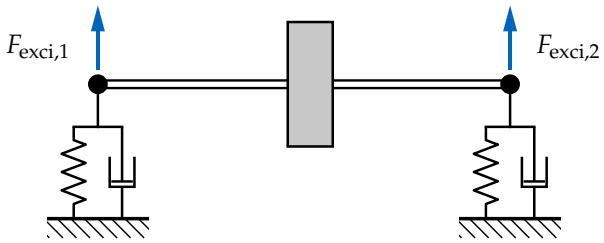

Figure 5. Model of the supported identified system using $\boldsymbol{F}_{\text{exci}}$ as input signal.

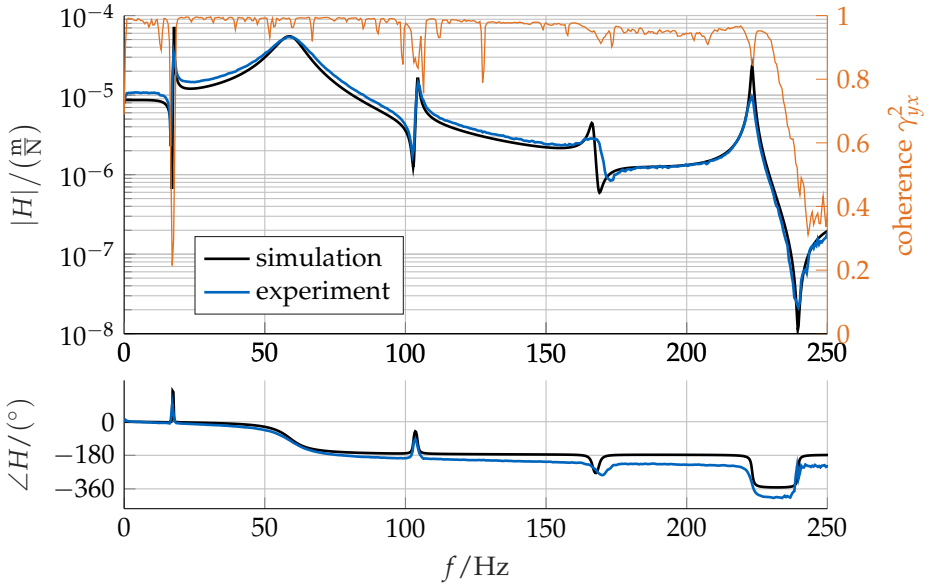

Figure 6. FRF H_{supp} of the rotor supported in magnetic bearings (using only excitation force), non-rotating.

Both curves show anti-resonances close to the resonance frequencies. This means, that the points for excitation or response measurement are very close to vibration nodes. This is due to the fact that the considered excitation and response locations for the measurements are directly at the AMB. The AMB's controller tries to minimize the displacement because it acts as a bearing. Naturally, the vibration nodes will be close to the bearing. The close vicinity of the excitation and measurement points to the bearing is a disadvantage of the method and can be interpreted as a bad observability and controllability at these points. The stiffer the AMBs are tuned, the worse the problem becomes.

This also means that the resulting FRFs are very sensitive to the exact positioning of the sensors as they are close to the vibration nodes. Small mistakes in the position have a rather large influence on the measured FRFs. So, an inherent problem of the method is that the excitation position is very close to the vibration nodes.

This experiment showed the measurement of the supported rotor FRF with a force estimation using only the additional excitation current.

3.2. FRF of the Free Rotor Using Total Force

In this section, the total force of the AMB is considered for the FRF calculation algorithm. Figure 7 shows the rotor that is cut free from the bearings.

The total force is estimated from Equation (5) and measured by the force platforms. It is the force that acts between the ground and the magnetic bearings. It includes the additional excitation force and the controller force. The controller force can be seen as the reaction force of the bearings. It is now assumed to be part of the external excitation and

the bearings are therefore no longer part of the characterized system. So, only the rotor without the bearings remains, i.e., the free rotor:

$$\boldsymbol{X}(\omega) \;=\; \boldsymbol{H}_{\text{free}}(\omega)\,\boldsymbol{F}_{\text{total}}(\omega) \tag{7}$$

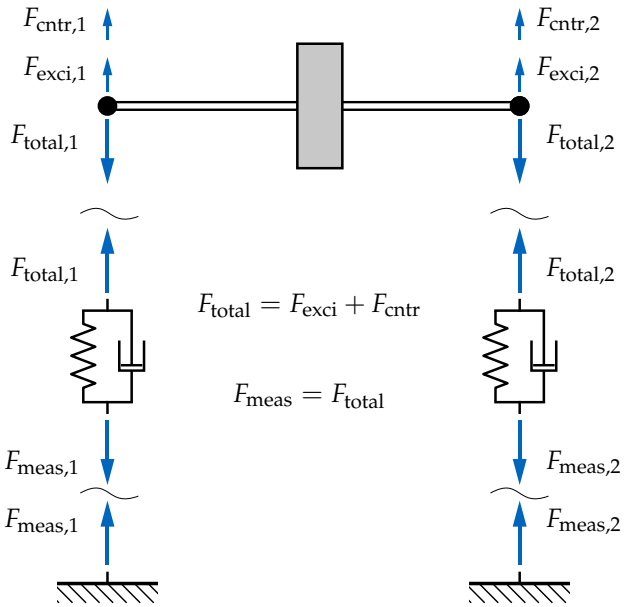

Figure 7. Model of the identified free system using the total force $\boldsymbol{F}_{\text{total}}$ as input signal.

For this example, the estimated total force is used and compared with the results from the measured total force. There are several methods to determine the total force. In [16], some possibilities are given. We summarize them in the order of increasing abstraction, i.e., starting from a method using a simple model to methods using more advanced models:

- Measuring the force between the AMB and the ground. This is applied here using the piezo force platforms as validation for the results involving a more complicated model. It is suggested to consider the inertia of the AMB. For this work, the inertia is not considered because the force platform is assumed to be rigid and rigidly fixed to the testbed.
- Measuring the magnetic flux density B using a Hall-sensor in the AMB and estimating the force using the area of the electromagnet and the magnetic permeability constant. This method enables the magnetic bearing to measure the total force, without using additional force sensors, making the AMB a self-sensing active component. It requires a simple model for the relationship between flux density B and the force F.
- Estimating the force from a more comprehensive model using the electrical current. This can be a model which has been parameterized experimentally or which used theoretical knowledge about the AMBs from an electromagnetic simulation model.
  One way is to directly measure the current. Current measurement is much cheaper and more easily available than, for example, force measurement.
  Another way is to estimate the current from the controller's output. The electrical current is not measured, but guessed from the control system's desired values. This is the method used in this work. It is assumed that the behavior of the electrical system is ideal, i.e., a desired current is perfectly executed. Here, the force is estimated using a linear static current–force relationship, given in Equation (5).

Figure 8 shows the results for the experimental FRF using the total force between the right magnetic bearing and the rightmost eddy current sensor. It shows the amplitude and phase of H_{free} and its coherence for the experimental results. This experimental FRF is obtained by using signals from the same experiment that was also described previously in Section 3.1. The curves *exp. measured total force* use the force that is directly measured by

the force platforms F_{meas}. The curves *exp. estimated force* use the force that is estimated from the total electric current $F_{\text{est,total}} = k_i \cdot I_{\text{total}}$. It is compared to the simulation results for the free rotor system.

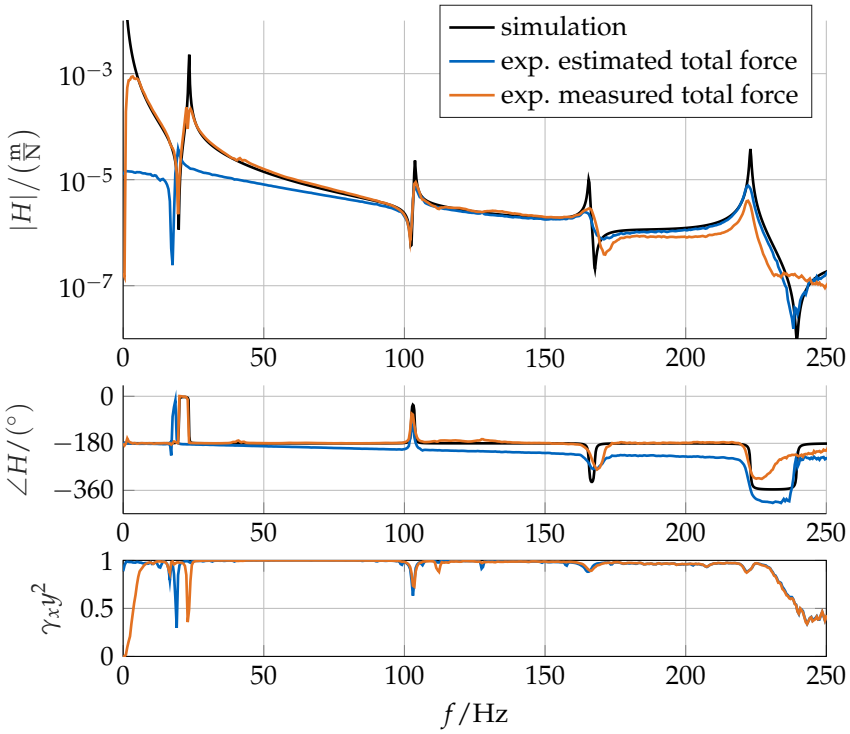

Figure 8. FRF H_{free} of the free rotor (using the total force), non-rotating, with coherence.

For the receptance FRF of a free system, one expects to see the effect of the rigid body modes, i.e., the amplitude starts at infinity, $|H(f \to 0)| \to \infty$. This can be clearly seen in the simulation results. In the experimental results, this is less obvious. For lower frequencies, the amplitude does not match. In order for the FRF to go to infinity, the FFT of the force must go to zero, as the displacement response is bounded by the bearings. A force FFT of zero is not possible in practice, as the force signal is then primarily dominated by noise. The same effect also applies to the resonance peaks with very high FRF amplitudes. The amplitude above 6 Hz and outside of the resonance points agrees very well using the force platforms, at least up to 210 Hz.

The FRF from the estimated force approaches the correct amplitudes only after approx. 90 Hz. The FRF with the estimated force is lower than for the measured force. This implies that the force is overestimated by the force estimation. The reason for the deviation in the amplitudes is not fully clear. It is suspected that the deviation is due to not considering the effect of the displacement on the magnetic force. Due to the bias current in the coils, the magnetic bearings have a destabilizing effect, i.e., they exhibit a negative stiffness that gives a force on the journal pulling it out of the center. The P-part of the PID-controller gives a positive stiffness that acts against the displacement. The controller force acts on the journal pointing towards the center, while the negative stiffness due to the bias current creates a force pointing away from the center. This can effectively decrease the bearing force. The effect of bias current on the out-of-center journal is not considered in the linear current–force estimation, thus creating an overestimation of the force.

As in the previous section, the simulation model agrees very well with the experimental result for the measured total force. For frequencies above 150 Hz, the simulation's damping is too low. This is caused by an imperfect model updating for the simulation model in Section 2.3.

The free rotor has vibration nodes close to the measurement positions, which makes the system sensitive to small positioning errors. In contrast to the previous section, this is

not an inherent problem of the method, but rather the case for this special rotor system, which has concentrated mass at the bearing journal while the rest of the rotor is rather slim.

Compared to the previous Section 3.1, there is no eigenfrequency at around 58 Hz, which was found from the identification of the rotor with supports because the FRF of the free rotor is determined here, using the total force.

The phase of the FRFs show a similar behavior between simulation and experiment.

The coherence has small dips at resonance points. This is especially relevant for the first peak. The same reason, which is given above, applies: the force is very low for high FRF amplitudes, so noise has a larger effect. In Figure 9, the ordinary coherence (correlation) between the input signals is shown. The controller force is dominant when there is large displacement that has to be controlled. At resonance frequencies of the supported system, the displacement is large and thus strongly influences the total force and thus its correlation. A high correlation of the input signals can cause problems in the FRF calculation due to the poor conditioning of the problem, cf. [2] (p. 327).

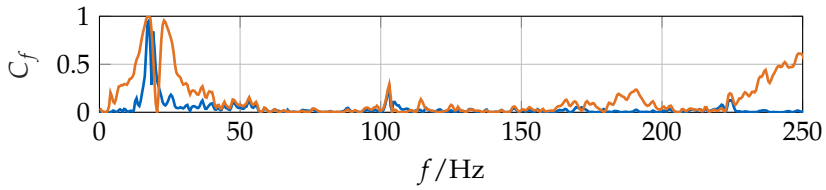

Figure 9. Ordinary coherence between the two input signals (total force).

Another effect that can negatively influence the results is internal feedback in the measured system. This can lead to biased FRFs, cf. [3]. In magnetic bearings, the displacement/position within the magnetic bearing directly influences the magnetic force. This influence was neglected in this contribution. For a significant feedback, disturbances in the output (displacement) have an effect on the input (force), which cannot be averaged out by the used H_1-estimator.

3.3. Interim Conclusions

It has been shown that it is possible to measure the FRF of the supported rotor system and of the free rotor in a single measurement run. The supported system's FRFs were experimentally determined by estimating the excitation force from the current, and the results agree well. The free rotor's FRFs were determined by considering the total force. The experimental results using the force estimation do not reflect the amplitude well for small frequencies. In the low frequency range, the estimation is insufficient. However, the overall behavior agrees well with simulation and experimental results using measured force.

The results for the FRFs using only force estimation showed differences in amplitude compared to simulation results or to measured force FRFs. In continuous condition monitoring, the FRFs (indicator function) of a rotating machine are continuously compared to previous FRFs. So, mostly differences in the FRFs are important, while the exact amplitude is of less importance, which supports the suitability of the presented FRF acquisition using estimated forces.

4. Rotating System—FRF of Free Rotor

In this section, an example of applying the measurement method to obtain the free rotor's FRF on the rotating system is presented shortly.

As given in Equation (2), in simulation, the FRF of a symmetric rotor at a given speed can be easily obtained from the system matrices. In contrast, experimental measurements of the FRFs for the rotating system are hard to acquire. Especially the FRF of the rotating free rotor cannot be obtained by usual EMA techniques, e.g., using impact testing.

Using the technique shown in this contribution, the rotor is excited in its magnetic bearings, and the total force is used for FRF-estimation. Figure 10 shows the determined FRFs

in simulation and from the experiment for a rotational speed of $\Omega = 800\,\text{rpm} \approx 13.3\,\text{s}^{-1}$. Two results from the experiment are shown.

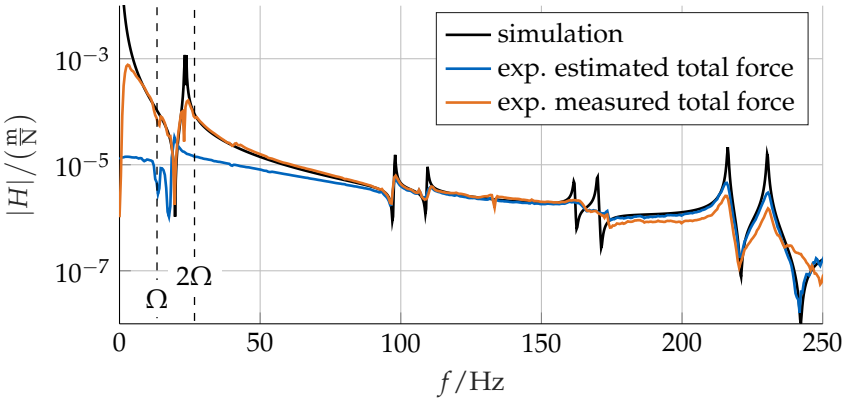

Figure 10. FRF amplitude $|H_{\text{free}}|$ of the free rotor (using total force) for 800 rpm.

The results are similar to Figure 8, with the damping of the simulation model still being too low. Due to the rotational speed, gyroscopic effects occur, which split the eigenfrequencies. This can be seen occurring in double peaks for the tilting modes.

At the frequency of rotation Ω and at 2 Ω, which are marked in the figure, the FRF with the measured force has a small dip. The disturbance at frequency Ω is due to unbalance. The unbalance force is not measured directly. However, the force is counteracted by both bearings and is thus indirectly measured. For a conventional impact excitation of the system, the additional unbalance force is not detected. That would lead to peaks in the FRF at multiples of the rotation frequency. Here, the unbalance force is indirectly measured. So, it cannot be predicted whether the FRF has a peak or a dip. The only possible statement is that the computed FRF should not be trusted for multiples of the rotation frequency. Outside of these critical points, the FRFs of the rotating system can be determined accurately with little disturbance from the rotation.

Figure 11 gives a summary of the experimentally determined FRFs. Each sub-figure shows the results from one measurement run, for 0 rpm and 800 rpm, respectively. This clearly shows the difference between the supported system's and free rotor's FRFs, where the rigid body modes are apparent at small frequencies for the free system and the distinct peak at around 58 Hz only appears in the supported system. By comparing the left and right parts of Figure 11, the splitting of eigenfrequencies with rotation becomes clear.

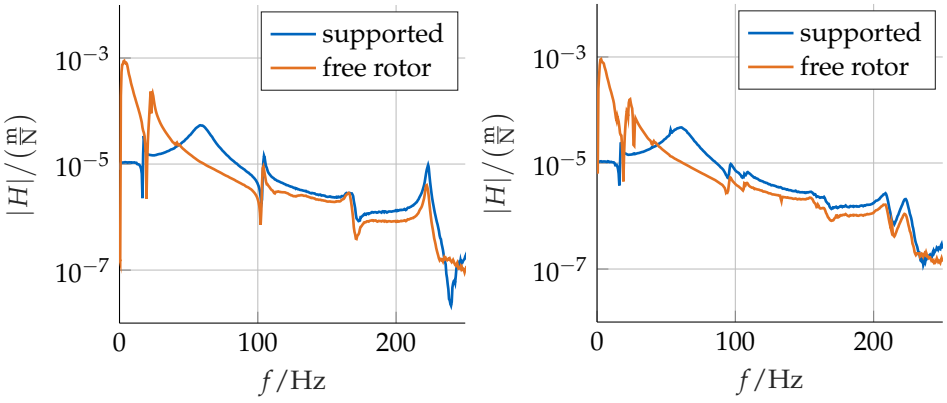

a. 0 rpm **b.** 800 rpm

Figure 11. Comparison of the experimentally determined FRFs for non-rotating and rotating system. The results for the supported system are obtained by considering the estimated excitation force. The results for the free rotor, shown here, use the measured total force.

Summary of Difficulties in the Experiments

Points that require special care in the experiments were given in this section for the rotating system and in the previous section for the non-rotating system. They are summarized here for convenience.

The biggest assumption in the method is the assumption of a linear current–force law with no influence from displacement. In combination with an imperfect calibration of the current-force factor k_i, this can lead to bias in the FRFs from estimated forces. The phase of FRFs from estimated forces show a linear drift, which was not compensated in the presented results. The correlation between input signals in the MIMO procedure must be checked to make sure that the results are valid. In the presented experiments, this was given in a large frequency region. When using results from measured forces, high FRF amplitudes cannot be accurately determined due to noise which pollutes measurements of very low forces. For FRFs with rotation, one must keep in mind that there is a pollution due to unbalance forces and higher harmonics at multiple of the rotation frequency.

5. Decoupling of Bearing Dynamics

This section gives a short outlook on a possible method to extract the bearing dynamics from FRF measurements of the supported system and free rotor. The resulting bearing dynamics could be used as indicator functions in a condition monitoring scheme.

Dynamic substructuring allows us to combine or decouple substructures, cf. [26,27]. Frequency-based substructuring uses frequency response functions of dynamic systems. The so-called dynamic decoupling uses dynamic stiffnesses, which are the inverse of frequency response functions $\boldsymbol{Z}(\omega) = \boldsymbol{H}^{-1}(\omega)$. Figure 12 shows the decoupling procedure to obtain the bearing dynamics. The free rotor is decoupled from the supported system, which yields the bearing dynamics, without the influence of the rotor itself. In primal decoupling, this is written as:

$$\boldsymbol{Z}_{\text{supp}}(\omega) - \boldsymbol{Z}_{\text{free}}(\omega) = \boldsymbol{Z}_{\text{AMB}}(\omega). \tag{8}$$

As an example, this procedure is applied on the results for the rotating system in Figure 10. For the supported system, the FRFs using the estimated excitation force are used. For the free rotor, the results from the estimated total force are used. Driving point FRFs in the middle of each the bearings are obtained by averaging the displacement signals from the eddy current sensors in the front and back plate of each bearing. Only the x-direction is considered because this is the direction of the excitation force. The rotor and bearing dynamics are taken to be axisymmetric.

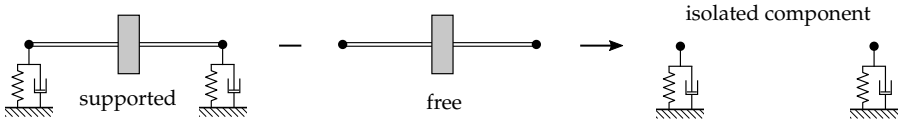

Figure 12. Decoupling procedure to obtain the dynamics of the bearings.

The dynamic stiffness matrix of the isolated AMB is the the result of the decoupling procedure, see Equation (8). The results of the decoupling are shown in Figure 13. The degrees of freedom are the x-directions in magnetic bearings 1 and 2. They are given as real and imaginary parts in sub-figures a and b, respectively.

For the real-part of $\boldsymbol{Z}_{\text{AMB}}$ in Figure 13a, the diagonal elements are close to a constant line, while the off-diagonal elements are close to zero. For the imaginary-part of $\boldsymbol{Z}_{\text{AMB}}$ in Figure 13b, the diagonal elements evolve approximately linear with the frequency, while the off-diagonal elements are again close to zero.

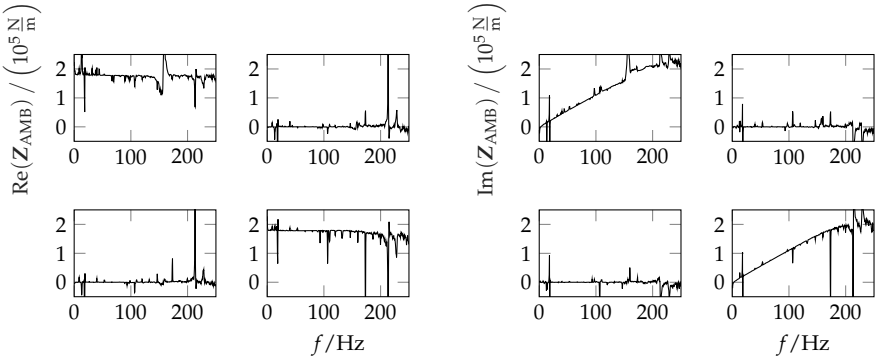

a. Real part **b.** Imagninary part

Figure 13. Decoupled $\boldsymbol{Z}_{\mathrm{AMB}}$ for 800 rpm, split in real and imaginary parts.

A simple dynamic model of the bearings can be used to model the system according to the experimental results for the dynamic stiffness of the isolated AMBs:

$$\boldsymbol{Z}_{\mathrm{AMB}} = \begin{bmatrix} k_{\mathrm{AMB},1} & 0 \\ 0 & k_{\mathrm{AMB},2} \end{bmatrix} + j\omega \begin{bmatrix} d_{\mathrm{AMB},1} & 0 \\ 0 & d_{\mathrm{AMB},2} \end{bmatrix}. \tag{9}$$

A simple curve fitting in the real and imaginary part can be used to obtain linear stiffness and damping of the bearings $k_{\mathrm{AMB},1}, k_{\mathrm{AMB},2}, d_{\mathrm{AMB},1}, d_{\mathrm{AMB},2}$. These identified parameters could be used in condition monitoring as indicators of the bearing condition. A large change in the bearings' stiffness and damping could indicate a fault in the bearings.

It should be noted that the identified parameters could only be used for monitoring purposes because of the uncertainties in the exact amplitude of the estimated FRFs. For condition monitoring, changes in the values are more important than exact calibrated absolute values. For a direct joint identification, high-quality FRFs would be needed with calibrated precise amplitudes.

6. Summary and Conclusions

This contribution shows that it is possible to measure the free FRF of a rotor and the supported system's FRF in a single measurement run using AMBs with multiple input signals. Measurement of the FRF of a rotating rotor without bearing influence could not be performed using usual impact hammer FRF measurements.

With the force estimator used in this contribution, the FRF amplitude cannot be accurately determined for low frequencies. For condition monitoring, the correct amplitude is not as critical as a continuous evaluation of the results. Thus, one could possibly use FRFs using estimated forces for condition monitoring.

The availability of FRFs of the free and the supported rotor during operation can further improve condition monitoring. It can be used to locate a possible fault. A fault in a bearing would show in the FRF of the supported rotor, but not in the FRF of the free rotor. A fault in a rotating component can be localized if it can be observed in both types of FRFs. A method to estimate the current bearing stiffness and damping was presented.

Furthermore, the possibility of measuring different FRFs during a machine's operation can be used to continuously adjust a machine model, i.e., for parameterizing a digital twin.

Free rotor FRFs can also be used to extend frequency-based substructuring, cf. [27], to rotating systems, which can, for example, be applied in experimental characterization of rotor system components (e.g., seals, journal bearings), see also Section 5. This requires high-quality FRFs, i.e., force measurement or an improved force-model.

Author Contributions: Conceptualization, M.K.; methodology, M.K.; software, M.K. and J.M.; validation, M.K.; formal analysis, M.K.; investigation, M.K.; resources, D.J.R.; data curation, M.K. and J.M.; writing—original draft preparation, M.K.; writing—review and editing, M.K., J.M., T.T. and D.J.R.; visualization, M.K.; supervision, T.T. and D.J.R. All authors have read and agreed to the published version of the manuscript.

Funding: This research received no external funding.

Institutional Review Board Statement: Not applicable.

Informed Consent Statement: Not applicable.

Data Availability Statement: Data available on request.

Conflicts of Interest: The authors declare no conflict of interest.

Abbreviations

The following abbreviations are used in this manuscript:

FRF	Frequency Response Function
AMB	Active Magnetic Bearing
EMA	Experimental Modal Analysis
MIMO	Multiple Input Multiple Output

References

1. Thümmel, T.; Rossner, M.; Wagner, C.; Maierhofer, J.; Rixen, D. Rotor Orbits at Operation Speed and Model-Based Diagnosis of Multiple Errors. In *Proceedings of the 10th International Conference on Rotor Dynamics—IFToMM*; Springer International Publishing: Cham, Switzerland, 2019; pp. 222–237. [CrossRef]
2. Brandt, A. *Noise and Vibration Analysis*; John Wiley & Sons, Ltd.: Chichester, UK, 2011. [CrossRef]
3. Bucher, I.; Ewins, D.J. Modal analysis and testing of rotating structures. *Philos. Trans. R. Soc. A Math. Phys. Eng. Sci.* **2001**, *359*, 61–96. [CrossRef]
4. Tiwari, R.; Lees, A.W.; Friswell, M.I. Identification of dynamic bearing parameters: A review. *Shock Vib. Dig.* **2004**, *36*, 99–124. [CrossRef]
5. De Santiago, O.C.; San Andrés, L. Field methods for identification of bearing support parameters—Part II: Identification from rotor dynamic response due to imbalances. *J. Eng. Gas Turbines Power* **2007**, *129*, 213–219. [CrossRef]
6. Zhou, J.; Di, L.; Cheng, C.; Xu, Y.; Lin, Z. A rotor unbalance response based approach to the identification of the closed-loop stiffness and damping coefficients of active magnetic bearings. *Mech. Syst. Signal Process.* **2016**, *66–67*, 665–678. [CrossRef]
7. Tiwari, R.; Lees, A.W.; Friswell, M.I. Identification of speed-dependent bearing parameters. *J. Sound Vib.* **2002**, *254*, 967–986. [CrossRef]
8. De Santiago, O.C.; San Andrés, L. Field methods for identification of bearing support parameters—Part I: Identification from transient rotor dynamic response due to impacts. *J. Eng. Gas Turbines Power* **2007**, *129*, 205–212. [CrossRef]
9. Numanoy, N.; Srisertpol, J. Vibration reduction of an overhung rotor supported by an active magnetic bearing using a decoupling control system. *Machines* **2019**, *7*, 73. [CrossRef]
10. Siva Srinivas, R.; Tiwari, R.; Kannababu, C. Application of active magnetic bearings in flexible rotordynamic systems—A state-of-the-art review. *Mech. Syst. Signal Process.* **2018**, *106*, 537–572. [CrossRef]
11. Ewins, D.J.; Robb, D.A.; Bucher, I.; Stanbridge, A.B.; von Groll, G.; Nordmann, R.; Reister, R.; Forth, P.; Schweitzer, G.; Gahler, C. *MARS—Modal Analysis of Rotating Structures: Development of Validated Structural Dynamic Modelling and Testing Techniques for Vibration Predictions in Rotating Machinery*; Technical Report; BRITE/EURAM Project no. 5464-92; Imperial College: London, UK, 1996.
12. Yang, R.; Tsunoda, W.; Han, D.; Zhong, J.; Shinshi, T. Frequency response function measurement of a rotor system utilizing electromagnetic excitation by a built-in motor. *J. Adv. Mech. Des. Syst. Manuf.* **2020**, *14*, JAMDSM0043. [CrossRef]
13. Chen, Y.; Yang, R.; Sugita, N.; Mao, J.; Shinshi, T. Identification of bearing dynamic parameters and unbalanced forces in a flexible rotor system supported by oil-film bearings and active magnetic devices. *Actuators* **2021**, *10*, 216. [CrossRef]
14. Matsubara, A.; Tsujimoto, S.; Kono, D. Evaluation of dynamic stiffness of machine tool spindle by non-contact excitation tests. *CIRP Ann.* **2015**, *64*, 365–368. [CrossRef]
15. Gähler, C.; Mohler, M.; Herzog, R. Multivariable identification of active magnetic bearing systems. *JSME Int. J. Ser. C Mech. Syst. Mach. Elem. Manuf.* **1997**, *40*, 548–592.
16. Förch, P.; Reister, A.; Gähler, C.; Nordmann, R. Modale Analyse an rotierenden Maschinen mittels Magnetlager. In *Schwingungen in Rotierenden Maschinen III*; Irretier, H., Nordmann, R., Eds.; Springer: Wiesbaden, Germany, 1995; pp. 245–254. [CrossRef]
17. Lee, C.w.; Ha, Y.H.; Joh, C.Y.; Kim, C.S. In-Situ Identification of Active Magnetic Bearing System Using Directional Frequency Response Functions. *J. Mech. Eng. Sci.* **1996**, *210*, 409–432. [CrossRef]

18. Maierhofer, J.; Gille, M.; Thümmel, T.; Rixen, D. Using the Dynamics of Active Magnetic Bearings to perform an experimental Modal Analysis of a Rotor System. In Proceedings of the 13th International Conference on Dynamics of Rotating Machinery (SIRM 2019), Copenhagen, Denmark, 13–15 February 2019. [CrossRef]
19. Maierhofer, J.; Thümmel, T.; Rixen, D.; Mechanik, A.; Maierhofer, J. Modellbasiertes Monitoring an magnetgelagerten Rotoren. In Proceedings of the SIRM 2017, Graz, Austria, 15–17 February 2017.
20. Kreutz, M.; Maierhofer, J.; Thümmel, T.; Rixen, D.J. Modaler Modellabgleich eines Rotors in Magnetlagern. In Proceedings of the Sechste IFToMM D-A-CH Konferenz, Lienz, Austria, 27–28 February 2020. [CrossRef]
21. Maierhofer, J.; Wagner, C.; Thümmel, T.; Rixen, D. Progress in Calibrating Active Magnetic Bearings with Numerical and Experimental Approaches. In *Mechanisms and Machine Science*; Springer: Cham, Switzerland, 2018; Volume 63, pp. 249–261. [CrossRef]
22. Schweitzer, G. Applications and Research Topics for Active Magnetic Bearings. In *IUTAM Symposium on Emerging Trends in Rotor Dynamics*; Gupta, K., Ed.; IUTAM Bookseries; Springer: Dordrecht, The Netherlands, 2011; Volume 1011. [CrossRef]
23. Brandt, A. ABRAVIBE—A MATLAB Toolbox for Noise and Vibration Analysis. 2019. Available online: www.abravibe.com (accessed on 26 April 2022).
24. GitHub: AMrotor—A MATLAB Toolbox for the Simulation of Rotating Machinery. Available online: https://github.com/AppliedMechanics/AMrotor (accessed on 26 April 2022).
25. Maierhofer, J.; Kreutz, M.; Mulser, T.; Thümmel, T.; Rixen, D.J. AMrotor—A MATLAB® Toolbox for the Simulation of Rotating Machinery. In *12th International Conference on Vibrations in Rotating Machinery*; Institute of Mechanical Engineers, Ed.; CRC Press: Liverpool, NY, USA, 2020. [CrossRef]
26. De Klerk, D.; Rixen, D.J.; Voormeeren, S.N. General framework for dynamic substructuring: History, review, and classification of techniques. *AIAA J.* **2008**, *46*, 1169–1181. [CrossRef]
27. van der Seijs, M.V.; de Klerk, D.; Rixen, D.J. General framework for transfer path analysis: History, theory and classification of techniques. *Mech. Syst. Signal Process.* **2016**, *68–69*, 217–244. [CrossRef]